New Journal of Physics
The open access journal at the forefront of physics

Deutsche Physikalische Gesellschaft DPG
IOP Institute of Physics

Published in partnership with: Deutsche Physikalische Gesellschaft and the Institute of Physics

OPEN ACCESS

RECEIVED
23 April 2016

REVISED
27 July 2016

ACCEPTED FOR PUBLICATION
15 August 2016

PUBLISHED
2 September 2016

PAPER

Picosecond laser filamentation in air

Andreas Schmitt-Sody[1], **Heiko G Kurz**[2], **Luc Bergé**[3], **Stefan Skupin**[4] **and Pavel Polynkin**[5]

[1] Air Force Research Labs, Kirtland Air Force Base, Albuquerque, New Mexico, USA
[2] Institute of Quantum Optics, Leibniz University Hannover, Welfengarten 1, D-30167 Hannover, Germany
[3] CEA-DAM, DIF, F-91297 Arpajon, France
[4] Univ. Bordeaux—CNRS—CEA, Centre Lasers Intenses et Applications, UMR 5107, 33405 Talence, France
[5] College of Optical Sciences, The University of Arizona, Tucson, Arizona, USA

E-mail: ppolynkin@optics.arizona.edu

Keywords: laser filamentation, picosecond laser pulses, nonlinear propagation, optical ionization

Abstract

The propagation of intense picosecond laser pulses in air in the presence of strong nonlinear self-action effects and air ionization is investigated experimentally and numerically. The model used for numerical analysis is based on the nonlinear propagator for the optical field coupled to the rate equations for the production of various ionic species and plasma temperature. Our results show that the phenomenon of plasma-driven intensity clamping, which has been paramount in femtosecond laser filamentation, holds for picosecond pulses. Furthermore, the temporal pulse distortions in the picosecond regime are limited and the pulse fluence is also clamped. In focused propagation geometry, a unique feature of picosecond filamentation is the production of a broad, fully ionized air channel, continuous both longitudinally and transversely, which may be instrumental for many applications including laser-guided electrical breakdown of air, channeling microwave beams and air lasing.

1. Introduction

Ionization of gases by powerful optical fields is one of the most important applications of intense pulsed lasers. Two specific interaction regimes have been particularly well studied. Ionization by nanosecond (ns) laser pulses, frequently termed optical breakdown, utilizes intense optical fields produced by *Q*-switched lasers [1] and has been investigated since the invention of laser *Q*-switching until the early 1980s [2]. In this context, experimental geometries with tight beam focusing are typically used. The physics associated with the gas response to the laser field is very complex as it involves numerous photochemical reactions, energy exchange between various particles and their mutual collisions [3, 4]. At the same time, the propagation of the ns laser field itself is usually treated in a simple way, e.g., by assuming particular temporal and spatial distributions for the laser intensity in the interaction zone. The second configuration involves intense femtosecond (fs) laser pulses. Here, at sufficiently high peak power of the pulse, Kerr self-focusing of the beam is counteracted by the defocusing action of plasma generated on the beam axis, resulting in the self-channeling propagation regime known as femtosecond laser filamentation [5, 6]. The temporal and spatial dynamics of the optical field are highly nonlinear [7–11]. However, these complex field dynamics are essentially decoupled from the rich air photochemistry driven by electron–particle collisions, as the latter happen on the time scales that are longer than the laser pulse duration. The disparity of the time scales for the field and plasma dynamics significantly simplify the analysis of femtosecond filamentation.

Compared to the ns and fs cases discussed above, the propagation of either collimated or weakly focused intense picosecond (ps) laser pulses in gaseous media has been studied to a much lesser extent. In the picosecond regime, both the highly nonlinear propagation of the laser pulse and the complex response of the gas impacted by electron–molecule and electron–ion collisions occur on comparable time scales. This is a very challenging regime to study not only numerically but experimentally as well, as high energies in the multi-Joule range are needed to drive significant avalanche ionization of the gas. Few works have been published on the subject. Most of them, with the exception of [12, 13], utilized ps laser pulses with rather low pulse energies (~mJ) in the UV

[14] or visible [15] spectral domains. The generated plasma densities with mJ-range pulse energies were much lower than what can be achieved with near-infrared Joule-level picosecond laser pulses, as we will show below.

In [12], near-IR ps laser pulses with tens of Joules of energy per pulse were used. The focus of that study was on the formation of multiple filaments within a collimated laser beam vertically launched into the atmosphere and on the generation of supercontinuum radiation. The peak intensity attained inside the individual filaments was argued to be similar to that in the fs regime. However, neither numerical simulations nor evaluations of the plasma densities were reported.

In a very recent publication [13], filamentation of laser pulses at 1.03 μm wavelength with fixed pulse duration of 1.5 ps was investigated experimentally and numerically. The numerical model neglected the effects of heating of the electron gas by assuming a constant electron-neutral collision time. The reported value of the clamped intensity was 23 TW cm^{-2}, which is very close to the result of our measurement and simulation for the particular pulse duration of 1.5 ps. Contrary to our results, a significant spectral broadening of the laser pulse, accompanied by pulse self-shortening, was observed. The likely explanation for the differences between our results and the results reported in [13] was that a significantly higher input pulse energies were used in our experiments, so that a fraction of the pulse energy was sufficient to singly ionize the entire nonlinearly interacting volume of air (1–10 J pulse energy in our case against 100 mJ used in [13]).

From the practical angle, studies in this field are motivated by various atmospheric applications such as air lasing [16], guidance of electrical discharges in air [17], lightning control [18] and channeling microwave beams [19]. Plasma produced through optical breakdown of air by tightly focused ns laser pulses is dense but spatially localized. By contrast, plasma channels produced through fs laser filamentation in air are extended and continuous, but they are dilute and short-lived, with plasma densities of 10^{16}–10^{17} electrons per cm^3 [20] and plasma lifetime of less than one nanosecond [21]. Attempts to combine the advantages of the fs and ns excitation regimes, through the use of the so-called igniter-heater scheme, have been shown to produce extended and dense plasma channels in air [22, 23]. However, plasma channels generated via the hybrid fs–ns excitation are usually fragmented into discrete plasma bubbles. All of the above shortcomings severely limit applications. In this paper, we report results of experiments and numerical simulations on the propagation of intense, weakly focused, ps laser pulses in ambient air. We show that all of the above-mentioned drawbacks of the ns, fs and the hybrid fs–ns regimes can be avoided through the use of energetic ps laser pulses, promoting robust, continuous and dense plasma columns in air.

2. Experimental setup and results

Our experiments make use of the Comet laser system which is a part of the Jupiter Laser Facility at the Lawrence Livermore National Laboratory in California, USA [24]. Comet is a chirped-pulse amplification chain based on Nd-doped glass. It produces 0.5 ps transform-limited pulses with maximum energy of 10 J per pulse, at the wavelength of 1.053 μm, in a 90 mm diameter beam. The laser operates in the single-shot regime (one shot in ten minutes). Laser pulses can be chirped up to 20 ps duration. To avoid the degradation of the 10 mm thick fused-silica exit window of the laser's vacuum compressor chamber, the peak laser power must not exceed 1 TW, which is more than one hundred times the critical power for self-focusing in air. Therefore, for pulses shorter than 10 ps, the laser energy is reduced accordingly. The laser beam is weakly focused in the ambient air using a 5 mm thick, 150 mm diameter meniscus lens with 3 m focal length.

In figure 1 we show a single-shot photograph of the plasma channel produced by a 10 J, 10 ps laser pulse. The ~30 cm long plasma string appears to be dense and longitudinally continuous, but the resolution of this image does not guarantee the transverse homogeneity of the plasma. The inset shows the fluorescence produced by the laser beam in far field, on a white paper screen. The image is taken through a color-glass filter that blocks the overwhelming light at the fundamental laser wavelength of 1.053 μm. Darker areas in the image result from the screening of the trailing edge of the laser pulse by the electron plasma generated on the leading pulse edge. The large dark area in the middle corresponds to the transversely continuous dense plasma on the beam axis. It is surrounded by several peripheral point-like plasma filaments. The production of a large-diameter plasma column that is not fragmented into multiple filaments may be compared to the 'superfilamentation' phenomenon recently discussed in connection with relatively tightly focused fs laser pulses [25]. The difference in the ps case discussed here is the important contribution of avalanche ionization, resulting in plasma densities significantly higher than those achievable in fs superfilaments.

It has been argued that the optical intensity in fs laser filaments in gases is clamped to a value that is independent of the energy of the laser pulse [26]. The clamping concept, which has been central in the fs filamentation science, is a consequence of the threshold-like dependence of the ionization yield and the associated nonlinear absorption on the optical intensity. Once the ionization threshold is reached, nonlinear absorption and plasma defocusing abruptly stop the further intensity buildup, which can be due to the nonlinear

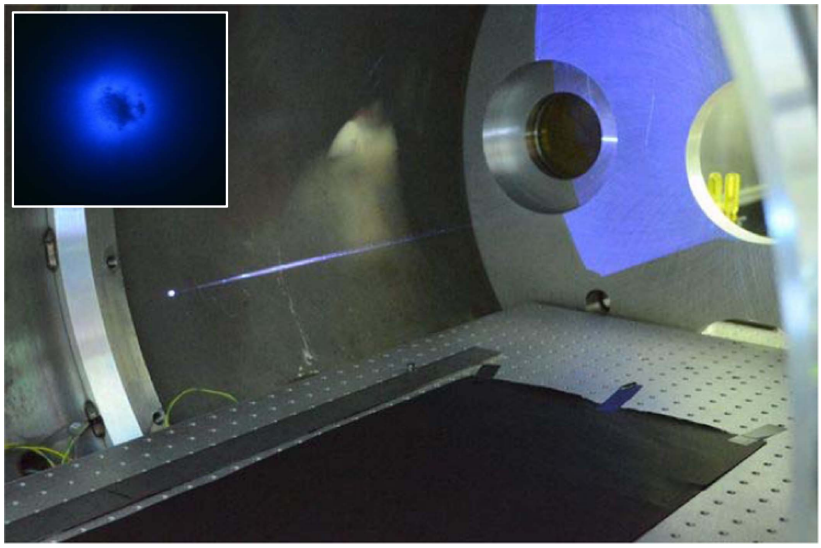

Figure 1. A photograph of the time-integrated fluorescence by the plasma column produced in air by a 10 J, 10 ps laser pulse, propagating from right to left and slightly downward. The inset shows fluorescence induced by the laser beam on a white paper screen placed in the far field. The dark area in the center of the image results from the screening of the trailing edge of the laser pulse by the dense and transversely uniform plasma channel.

self-focusing or linear focusing by an external focusing optic of both. Although this description is somewhat oversimplified as it does not account for the complex temporal pulse dynamics in fs filaments, the concept of intensity clamping works very well for fs pulses (with the exception of the short temporal spikes that may develop on the trailing edge of the pulse; those spikes, however, carry only a small fraction of the total energy of the laser pulse [27]). The reason is that the relevant ionization rates and thus the generated plasma densities depend very sharply on the pulse intensity (i.e., $\propto I^{11}$), while the dependence of the plasma density on the pulse duration is only linear. Therefore, the exact shape of the pulse, in particular its duration, are of a lesser importance than the value of the peak intensity, as long as the pulse remains ultrashort. In the case of ps pulses, where avalanche ionization provides a major contribution to plasma generation, the validity of the intensity clamping concept is not *a priori* obvious. It may be more appropriate to talk about clamping of the fluence, which is the integral of the intensity over the whole pulse and, importantly, provides a direct physical observable.

In the case of ps pulses, the temporal intensity buildup is much slower that in the fs case. As our simulations will show, the temporal and spatial dynamics of energetic ps pulses are decoupled, and the temporal pulse shape remains weakly distorted. That conclusion is experimentally supported by the measurements of spectra of the laser pulses after passing through the filamentation zone. The measurements show almost no spectral broadening, i.e. no significant distortions of the pulse shape, up to the highest level of the pulse energy used in the experiments. If no significant temporal reshaping of the pulse occurs on propagation, the notions of intensity and fluence clamping are equivalent.

In order to evaluate the fluence of the ps laser field in the interaction zone we produce single-shot ablation of the front surface of a glass slide placed along the beam path close to the position of maximum plasma production. This position is determined as the point with the brightest plasma fluorescence on a photographic image of the plasma string (similar to figure 1). The ablation pattern marks a circular region with a sharp boundary, inside which the laser fluence exceeds the threshold value for surface ablation of the glass (see figure 2). We have separately measured the ablation threshold fluence for the particular type of glass we used (soda-lime glass microscope slides), for near-infrared laser pulses with various durations in the range from 1 to 10 ps. We found that the ablation threshold fluence steadily grows with pulse duration in that range, from 2.5 to 5 J cm^{-2}.

Data for the diameter of the ablation mark versus pulse energy, for the case of 10 ps pulse, are shown in figure 2. The corresponding area of the mark, which is proportional to the diameter squared, scales linearly with the pulse energy, as evidenced by the agreement of the data with the dashed regression curve. Thus, the average fluence computed as the ratio of the pulse energy to the ablation area is approximately constant (or clamped) with respect to the pulse energy, at a given pulse duration. We have conducted these measurements using laser pulses with different durations and found that the average laser fluence was clamped in all cases. The actual value of the clamped fluence was found to be a growing function of the pulse duration, as shown in figure 3(a).

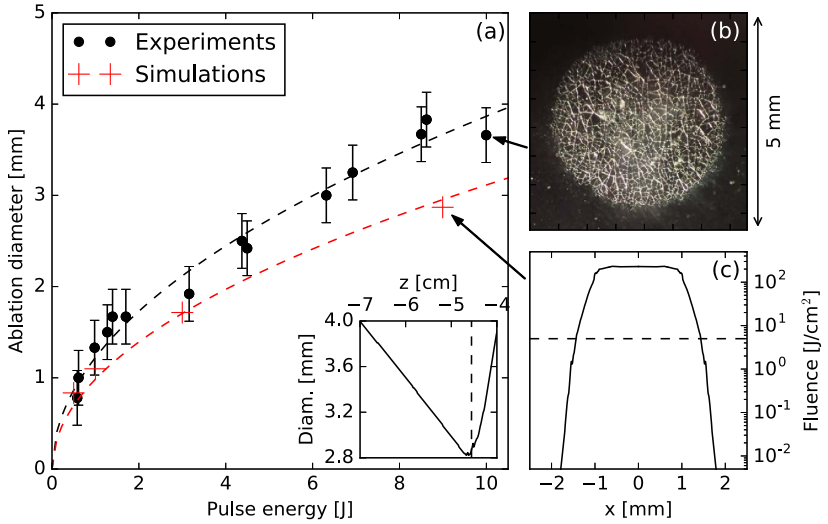

Figure 2. (a) Measured (•) and simulated (+) diameters of ablation marks produced by 10 ps pulses with various energies on a glass surface placed at the position of peak air ionization. The dashed curves are fits proportional to the square-root of the pulse energy. (b) Photograph of the ablation mark produced by a 10 J, 10 ps pulse. (c) The simulated fluence profile for a 9 J, 10 ps pulse. The 5 J cm^{-2} level corresponding to the ablation threshold fluence for 10 ps pulse duration is marked with a dashed line. The inset in (a) shows the simulated beam diameter at the ablation threshold level of 5 J cm^{-2} versus the distance from the geometrical focus for a 9 J, 10 ps pulse.

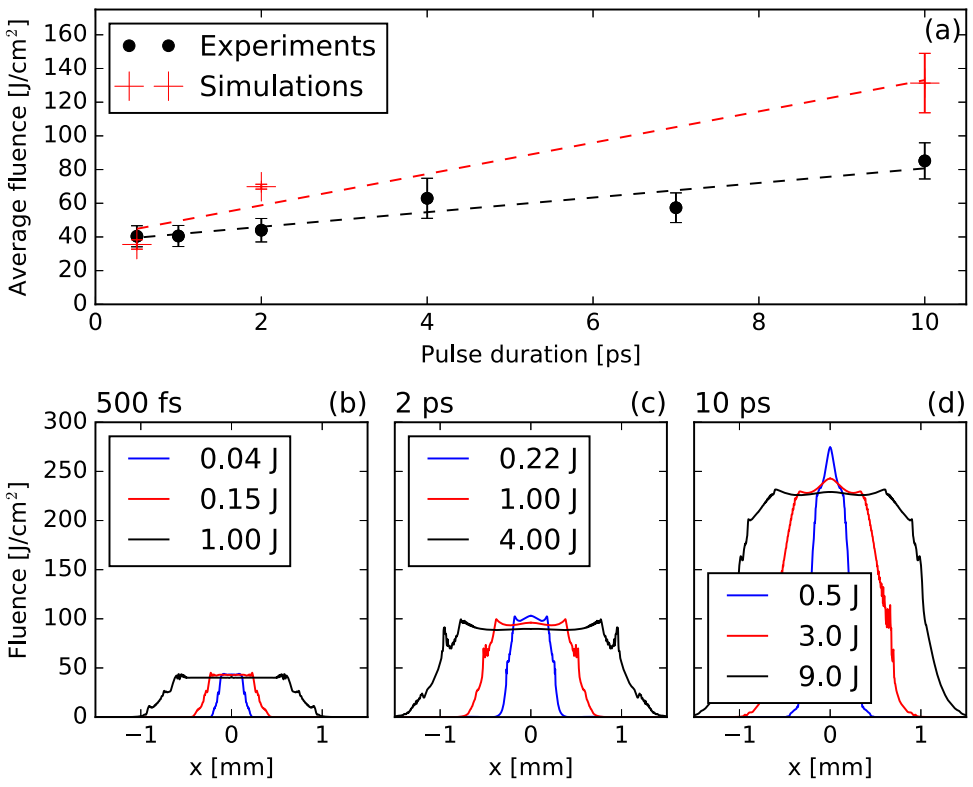

Figure 3. (a) Measured (•) and simulated (+) average laser fluence at the position of peak air ionization, versus pulse duration. At any given pulse duration, the average fluence is clamped, i.e., approximately independent of the pulse energy. Error bars are computed from deviations from the regression curves (i.e., see figure 2(a)). (b)–(d) Computed fluence profiles at the positions of peak ionization, for various pulse configurations, showing fluence clamping.

The density of plasma in the ionized channel has been experimentally evaluated using a capacitive plasma probe setup. The details of this characterization technique are discussed in [28]. In this particular case, the probe has two 5 cm long electrodes separated by a distance of 3 cm and charged to a voltage of 50 V. The signal produced by the probe in our experiments is five to six orders of magnitude higher than the signal from the same

probe applied to a regular femtosecond plasma filament with an independently known plasma density between 10^{16} and 10^{17} cm^{-3} [20]. Accounting for the difference in the total volumes of the plasma detected by the probe in the picosecond case under investigation and that of the known reference femtosecond filament, our measurements indicate a complete or nearly complete single ionization of air by the picosecond pulse in the interaction zone. The uniformity of plasma fluorescence, inferred from the single-shot photographic images, indicates that the plasma is longitudinally uniform along the ionized channel.

Although the above plasma probes have been applied for plasma characterization in laser sparks and filaments in gases for many years [1, 29, 30], we point out, following [28], that such a characterization technique is at best semi-quantitative. These probes do not detect free electrons directly, as electrons attach to neutral oxygen molecules in the air on a much faster time scale than what it would take for the electrons to drift towards the probe's electrodes. Instead, the probe detects negative O_2^- complexes and positive oxygen and nitrogen molecular ions that have much longer lifetimes than the lifetime of free electrons. The measurements with such probes also depend on the electron plasma temperature that, in turn, determines the plasma dynamics. Therefore, these measurements are only good for rough order-of-magnitude evaluations of air-plasma density.

3. Numerical simulations

3.1. The time-dependent model

For numerical simulations of our experiments we have devised a model that combines a unidirectional nonlinear pulse propagator for the laser field amplitude U [31] with a material response module. The unidirectional treatment is valid as the estimated peak reflectivity of the plasma is less than 10^{-4}, even assuming a complete single ionization of all air molecules. Our model accounts for multiphoton, tunnel, and impact single ionization of oxygen and nitrogen molecules with the initial densities of $\rho_{N_2}^{(0)} = 2.2 \times 10^{19}$ cm^{-3} and $\rho_{O_2}^{(0)} = 5.4 \times 10^{18}$ cm^{-3}, respectively. Direct photoionization via Perelomov, Popov and Terent'ev (PPT) theory [32] is included for oxygen molecules only, as the ionization potential of oxygen is lower than that of nitrogen. Collisional ionization is included for both neutral species. To that end, we compute the inverse bremsstrahlung heating of free electrons using the electron temperature-dependent collision rates

$$\nu_{O_2^+}(T_e) = 7 \times 10^{-6} \rho_{O_2^+}[\mathrm{cm}^{-3}](T_e[\mathrm{eV}])^{-3/2}\ \mathrm{s}^{-1}, \tag{1}$$

$$\nu_{O_2}(T_e) = 2 \times 10^{-7} (\rho_{O_2}^{(0)}[\mathrm{cm}^{-3}] - \rho_{O_2^+}[\mathrm{cm}^{-3}])(T_e[\mathrm{eV}])^{1/2}\ \mathrm{s}^{-1}, \tag{2}$$

$$\nu_{N_2^+}(T_e) = 7 \times 10^{-6} \rho_{N_2^+}[\mathrm{cm}^{-3}](T_e[\mathrm{eV}])^{-3/2}\ \mathrm{s}^{-1}, \tag{3}$$

$$\nu_{N_2}(T_e) = 2 \times 10^{-7} (\rho_{N_2}^{(0)}[\mathrm{cm}^{-3}] - \rho_{N_2^+}[\mathrm{cm}^{-3}])(T_e[\mathrm{eV}])^{1/2}\ \mathrm{s}^{-1} \tag{4}$$

in the respective collision cross-sections $\sigma_X = e^2 \nu_X(T_e)/m_e \epsilon_0 n_0 c \omega_0^2$ [33] (subscript X indexes different molecular and ionic species: N_2, N_2^+, O_2 and O_2^+). Our nonlinear propagator model reads as follows:

$$\frac{\partial}{\partial z} U = \frac{\mathrm{i}}{2k_0} \hat{T}^{-1} \nabla_\perp^2 U + \mathrm{i}\hat{\mathcal{D}} U + \mathrm{i}\frac{\omega_0}{c} n_2 \hat{T} R * |U|^2 U$$
$$- \mathrm{i}\frac{k_0}{2n_0^2 \rho_c} \hat{T}^{-1} \rho_e U - \frac{\sigma_e}{2} \rho_e U - \frac{E_{O_2} W_{O_2}^{\mathrm{PPT}}(|U|^2)}{2|U|^2} (\rho_{O_2}^{(0)} - \rho_{O_2^+}) U, \tag{5}$$

$$R(t) = \frac{1}{2}\delta(t) + \frac{1}{2}\Theta(t) \frac{\tau_1^2 + \tau_2^2}{\tau_1 \tau_2^2} e^{-t/\tau_2} \sin(t/\tau_1), \tag{6}$$

$$\frac{\partial}{\partial t} \rho_{O_2^+} = W_{O_2}^{\mathrm{PPT}}(|U|^2)(\rho_{O_2}^{(0)} - \rho_{O_2^+}) + \frac{\sigma_{O_2}}{E_{O_2}} \rho_e |U|^2, \tag{7}$$

$$\frac{\partial}{\partial t} \rho_{N_2^+} = \frac{\sigma_{N_2}}{E_{N_2}} \rho_e |U|^2, \tag{8}$$

$$\frac{\partial}{\partial t} T_e = \frac{2}{3k_B} \sigma_e |U|^2$$
$$- \left(\frac{T_e}{E_{O_2}} + \frac{2}{3k_B} \right) \sigma_{O_2} |U|^2 - \left(\frac{T_e}{E_{N_2}} + \frac{2}{3k_B} \right) \sigma_{N_2} |U|^2. \tag{9}$$

Here, we use the conventional notation for fundamental constants; ω_0 is the laser angular frequency, n_0 is the corresponding linear refractive index of air, $k_0 = \omega_0 n_0 / c$ is the wavenumber, ρ_c is the critical plasma density and $\rho_e = \rho_{O_2^+} + \rho_{N_2^+}$ is the free-electron density. The operator $\hat{T}$ accounts for the self-steepening and space–time focusing effects [34]. Linear dispersion of air is included in equation (5) via the operator $\hat{\mathcal{D}}$ [35]. For the value of the nonlinear refractive index of air we use $n_2 = 2.8 \times 10^{-19}$ cm^2 W^{-1} [36]. For generality, we equally

partition n_2 into the instantaneous and delayed contributions according to equation (6) with $\tau_1 = 60$ fs and $\tau_2 = 80$ fs, although the delayed rotational contribution to nonlinearity is indistinguishable from the instantaneous nonlinear response for picosecond pulses. E_{N_2} and E_{O_2} are the ionization potentials of the neutral nitrogen and oxygen molecules, respectively. The compound collision cross-section is defined as $\sigma_e = \sigma_{O_2^+} + \sigma_{N_2^+} + \sigma_{O_2} + \sigma_{N_2}$. Electron recombination and attachment to neutral molecules are neglected as the time scales for those processes are much longer than the pulse duration.

We point out that in a recent publication [37] the value of 3.9×10^{-19} cm^2 W^{-1} was reported for the effective (instantaneous plus delayed) nonlinear refractive index of air, which is higher than the value that we use in our simulations. We checked that using the two different values of n_2 in the simulation of our experiment yields essentially identical results, as the linear focusing with the lens, under our experimental conditions, produces a significant, if not dominant, contribution to the effective net focusing of the beam. We also checked that accounting for the depletion of neutrals in the Kerr term and photoionization of N_2 using the corresponding PPT rate in equation (8) does not appreciably change the results of our simulations.

Results of our numerical simulations are shown in figures 2 and 3, together with their experimental counterparts. The simulations used here utilize an axially symmetric implementation of the model discussed above. In order to mimic the experimental conditions, we use Gaussian temporal $\propto \exp(-t^2/t_0^2)$ and super-Gaussian spatial $\propto \exp(-r^4/w_0^4)$ profiles for the input laser field. Simulations start 8 cm before the position of the geometrical focus, where intensities do not exceed 10 TW cm^{-2} and ionization is still negligible. The code propagates the focused pulse, finds the longitudinal position of maximum air ionization and, at that position, computes the diameter of the area inside which the fluence exceeds the ablation threshold value (e.g., 5 J cm^{-2} for the case of 10 ps pulse). Simulation results for the size of ablation agree with experiments within about 25%. The experimental ablation marks may be larger than the computed ones because of (i) the beam defects that are not accounted for in the model; (ii) the uncertainty of the longitudinal placement of the glass sample, estimated as ± 0.5 cm. From the simulated beam diameter at the 5 J cm^{-2} level versus longitudinal position shown in the inset of figure 2(a), it is clear that the placement uncertainty may affect the measurement significantly. In contrast, the uncertainty of the value of the ablation threshold should not significantly affect the computed diameter of the ablation mark due to the sharp spatial gradients of the fluence profile.

In figure 3(a) we show the average fluence, defined here as a ratio of the pulse energy to the area of the beam with fluence above the corresponding ablation threshold value. Numerical and experimental data agree reasonably well and both show a steady growth of the average fluence with pulse duration. For both numerical and experimental data, the error bars are computed from the deviations of the data points from the square-root regression curves, shown in figure 2(a) with the dashed lines for the case of 10 ps pulses. While we report an almost perfect linear dependence of the simulated ablation area on the pulse energy for shorter pulses (not shown), some deviation from linearity is evident for the case of 10 ps pulses. The inspection of the computed fluence profiles (figures 3(b)–(d)) confirms fluence clamping. Note that the value of the clamped fluence for the 1.5 ps input pulse duration is about 40 J cm^{-2}. Assuming that the pulse duration does not significantly change on propagation, which is supported by simulations and measurements of the very small spectral broadening of the laser pulse after the filamentation zone, the corresponding value of the clamped intensity is about 25 TW cm^{-2}. That number is very close to the peak intensity level of 23 TW cm^{-2} reported in [13] for 100 mJ, 1.5 ps long laser pulses.

Simulations show a complete single ionization of both oxygen and nitrogen molecules in the ps filament, confirming the results of the semi-quantitative measurements using the capacitive plasma probe discussed above. Computed plasma density exceeds 10^{19} cm^{-3} for a wide range of pulse energies and durations. Figures 4(a) and (b) show the distributions of plasma produced by 500 fs and 10 ps pulses, each with 1 J of energy. While the shorter pulse produces plasma near the beam axis only, the 10 ps pulse produces a much larger, homogeneous plasma channel with complete single ionization of air molecules. Electron temperatures up to 35 eV are achieved with 1 J pulses in the region of complete ionization, as shown in figure 4(c). With 10 J pulses, electron temperatures as high as 100 eV are observed. The inspection of the spatio-temporal intensity profiles (two snapshots are shown in figure 4(d)) reveals that a complete single ionization of air, predominantly through collisional ionization, occurs on the leading edge of the pulse, which remains relatively intact with intensity clamped at the level below 100 TW cm^{-2}.

3.2. The time-averaged model

The simulations discussed so far utilized an axially symmetric implementation of our model, because fully space and time resolved simulations of ps pulses would be prohibitively expensive in terms of computational resources. Thus, based on the above data we cannot rule out the possible onset of multiple filamentation, which may break the plasma channel in the transverse plane. To investigate the transverse uniformity of the plasma column, which is evident from our experimental results, we conduct another set of simulations employing a spatially full 3D (x, y, z) but time-integrated version of equation (5). To be able to formulate a closed-form,

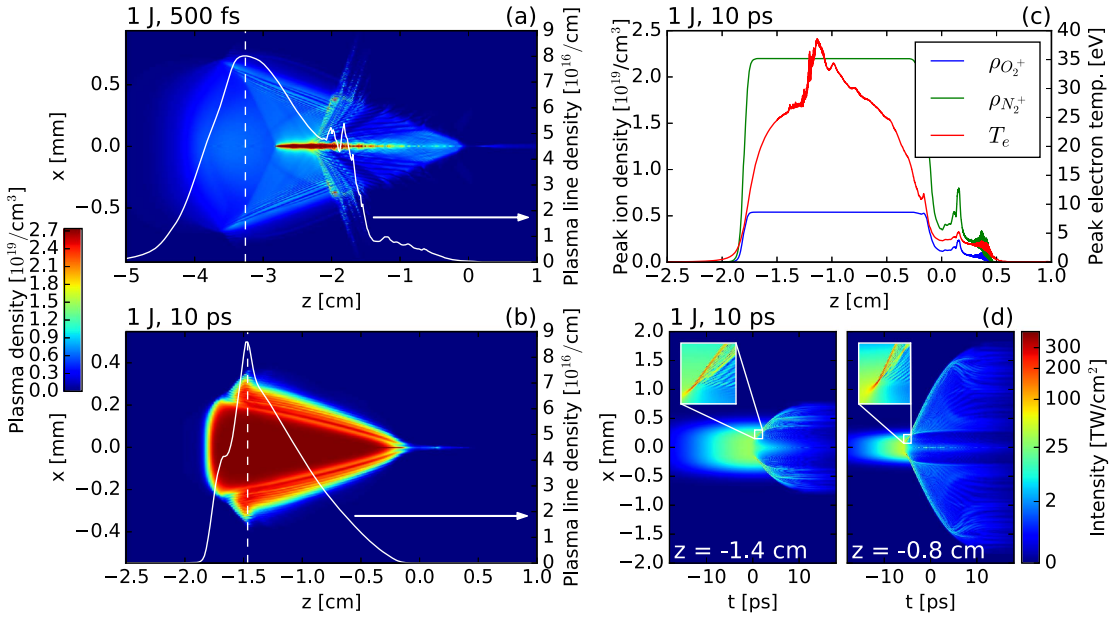

Figure 4. (a) Simulated plasma channel produced by a 500 fs, 1 J laser pulse. The longitudinal position of the peak plasma production (the maximum of the linear plasma density $\int \rho_e(r, z, t) r \mathrm{d}r$ for t larger than the pulse duration) is marked by the dashed white line. (b) Same for a 10 ps pulse with 1 J energy. (c) Peak ionic densities and electron temperature versus propagation distance for the 10 ps pulse shown in (b). (d) Snapshots of the corresponding spatio-temporal intensity profiles. All longitudinal coordinates are shown with respect to the linear geometrical focus of the focusing lens.

time-integrated version of equation (5), we resort to the following set of approximations, all of which are justified, provided that we are only interested in a qualitative conclusion on whether the transverse beam instability is strong enough to cause multi-filamentation. First, the possible onset of multi-filamentation, should multi-filamentation occur, will happen along the self-focusing stage of propagation, prior to the onset of significant ionization, which would tame rather than enhance the instability. Should the multi-filamentation occur, it will be seeded by the spatial non-uniformities of the initial transverse beam profile. Accordingly, we simulate broad realistic beams by approximating their time dependence by a Gaussian pulse profile and discard air dispersion. Further, we restrict plasma generation to multiphoton ionization of oxygen molecules at the rate $W_{O_2} = \sigma_{11}|U|^{22}$ with the 11-photon cross-section $\sigma_{11} = 2 \times 10^{-4}\,\mathrm{s^{-1}cm^{22}\,TW^{-11}}$. By doing so, we systematically underestimate plasma generation, as we neglect both multi-photon ionization of nitrogen molecules and avalanche ionization of both oxygen and nitrogen molecules. Consequently, we overestimate self-focusing and the corresponding transverse modulation instabilities. As our results will show, even in that case the filament remains transversely uniform. Therefore the account for avalanche ionization, which could only mitigate the transverse instability, would not change the qualitative conclusion on the transverse uniformity of the plasma filament.

Following [38], the field envelope is decomposed as $U = \psi(x, y, z) \times \exp(-t^2/t_0^2)$, where t_0 corresponds to the initial pulse duration. Then we find $\rho_{O_2^+}(t) \approx \gamma_{O_2^+}|\psi|^{22}\,[\mathrm{erf}(\sqrt{22}\,t/t_0) + 1]$, where $\mathrm{erf}(x)$ denotes the usual error function and $\gamma_{O_2^+} = \sqrt{\pi/88}\,t_0\sigma_{11}\rho_{O_2}^{(0)}$. After plugging the above expressions into equation (5), multiplying the entire equation with the pulse profile $\propto\exp(-t^2/t_0^2)$, and integrating the propagation equation over the entire time domain, we arrive at the following extended nonlinear Schrödinger equation for the spatial profile $\psi(x, y, z)$ accounting for self-focusing, plasma defocusing, and multiphoton absorption:

$$\frac{\partial}{\partial z}\psi = \frac{\mathrm{i}}{2k_0}\nabla_\perp^2\psi + \mathrm{i}k_0\left(\alpha n_2|\psi|^2 - \frac{\gamma_{O_2^+}}{2\rho_c}|\psi|^{22}\right)\psi - \frac{E_{O_2}\sigma_{11}\rho_{O_2}^{(0)}}{2\sqrt{11}}|\psi|^{20}\psi. \tag{10}$$

For pulse durations much larger than the dephasing time, $t_0 \gg \tau_2$ (see equation (6)), the contribution of the delayed Raman response to self-focusing is indistinguishable from the instantaneous Kerr response, and we find $\alpha \approx 1/\sqrt{2}$. An extended version of this model has been shown to faithfully reproduce experimental beam patterns in multifilamentation of fs pulses with peak power significantly above critical [38, 39].

The beam profile for the laser source used in our experiments has not been characterized because of its extremely low firing rate. In order to numerically investigate the potential multifilamentation dynamics for our ps pulses, we instead used two different representative input beam shapes: (i) a noisy fluence profile characteristic of multi-Terawatt fs lasers [38, 39]; in that case small-scale transverse fluctuations of the beam

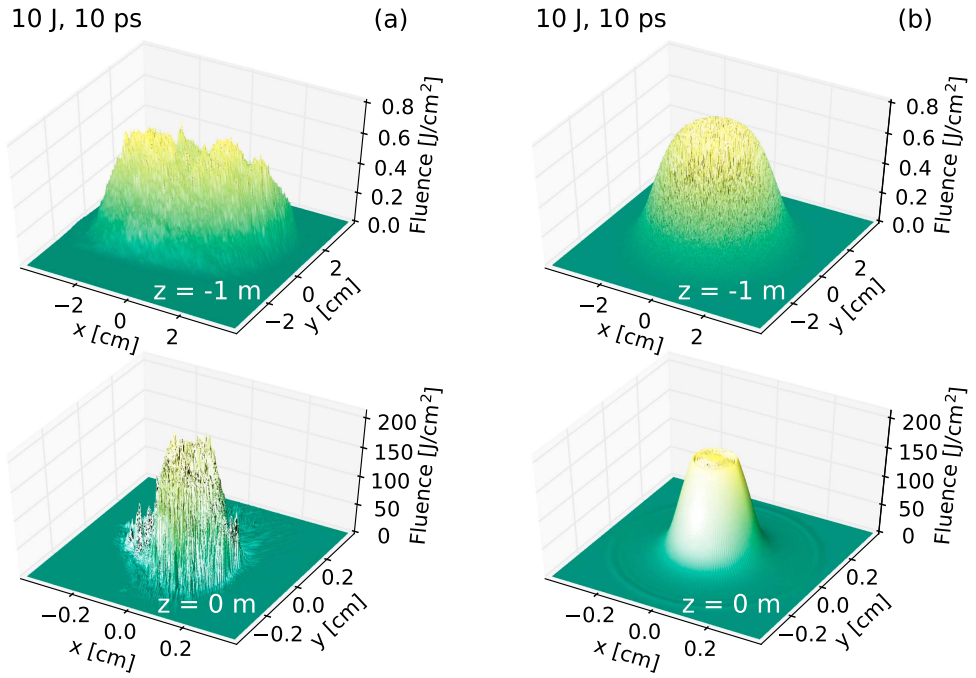

Figure 5. Fluence profiles computed using the time-integrated propagation model equation (10) and (a) a realistic noisy input beam and (b) a 4th order super-Gaussian input fluence profile perturbed by 10% amplitude random noise (see text for details). In both cases, the beam profiles 1 m before and at the linear focal plane are shown in the top and bottom panels, respectively.

fluence can efficiently seed the transverse modulation instability, and (ii) a 4th-order super-Gaussian beam profile perturbed by the addition of 10% of random amplitude noise. Figure 5 shows the fluence distributions produced by such input beam profiles for 10 J, 10 ps pulses. The simulations are started 1 m before the position of the geometrical focus, where intensities are about 0.1 TW cm^{-2} and nonlinear effects are negligible. Near focus, maximum intensities reach tens of TW cm^{-2}. For such intensities, analytical estimates suggest that the instability growth rate, $\Gamma = k_0(\alpha n_2 I - 11\gamma_{O_2^+} I^{11}/2\rho_c)$, of stationary transverse modulations [40] satisfy $\Gamma < 0$ so that transverse perturbations are not amplified. Thus, a broad plasma channel, once formed, does not have tendency to breakup into multiple filaments. On the propagation stage towards the nonlinear focus, intensities are lower, e. g., $I \leqslant 1$ TW cm^{-2}, and small-scale beam fluctuations cannot grow on the scale of our experiments. Thus, experimental results, analytical estimates and numerical simulations all show that under our experimental conditions, no breakup of the beam into multiple filaments occurs on propagation and the plasma channel remains transversely uniform. We point out that the role of the external linear focusing in the propagation dynamics of ultraintense ps pulses remains to be quantified; it is likely to contribute to the inhibition of multi-filamentation, similar to the case of 'superfilamentation' mentioned above. Also note that in the simulation using the noisy input beam (figure 5(a)), several peripheral smaller filaments emerge outside the plasma region, in agreement with the experimental observations (see the inset in figure 1).

4. Conclusion

In conclusion, we have investigated the propagation of TW, ps laser pulses in air by means of experiments and numerical simulations. Our model is based on a unidirectional pulse propagator coupled to a material response module that accounts for multiphoton, tunnel and impact ionization of air molecules, as well as heating of electron plasma. We report good agreement between experimental and numerical results. Our major finding is the possibility to produce a broad, fully ionized, as well as longitudinally and transversely continuous channel, that can be instrumental for various atmospheric applications such as the guidance of DC electrical breakdown of air, channeling microwave beams and air lasing.

Acknowledgments

This material is based upon work supported by the US Defense Threat Reduction Agency under program number HDTRA 1-14-1-0009 and by the US Air Force Office of Scientific Research under programs number

FA9550-12-1-0482 and number FA9550-16-1-0013. The use of the Jupiter Laser Facility was supported by the US Department of Energy, Lawrence Livermore National Laboratory, under contract no. DE-AC52-07NA27344. Numerical simulations were performed at Mésocentre de Calcul Intensif Aquitain (MCIA), Grand Equipement National pour le Calcul Intensif (GENCI, supported under grants no. 2015-056129 and 2016-057594), and The Partnership for Advanced Computing in Europe (PRACE, supported under grant no. 2014-112576). LB thanks Patrick Combis for the discussions on ablation thresholds in glasses.

References

[1] Meyerand R G and Haught A F 1963 Gas breakdown at optical frequencies *Phys. Rev. Lett.* **11** 401
[2] Bekefi G (ed) 1976 *Principles of Laser Plasmas* (New York: Wiley)
[3] Raizer Y P 1991 *Gas Discharge Physics* (Berlin: Springer)
[4] Itikawa Y, Ichimura A, Onda K, Sakimoto K, Takayanagi K, Hatano Y, Hayashi M, Nishimura H and Tsurubuchi S 1989 Cross sections for collisions of electrons and photons with oxygen molecules *J. Phys. Chem. Ref. Data* **18** 23
[5] Couairon A and Mysyrowicz A 2007 Femtosecond filamentation in transparent media *Phys. Rep.* **441** 47
[6] Bergé L, Skupin S, Nuter R, Kasparian J and Wolf J P 2007 Optical ultrashort filaments in weakly-ionized, optically-transparent media *Rep. Prog. Phys.* **70** 1633
[7] Champeaux S and Bergé L 2003 Femtosecond pulse compression in pressure-gas cells filled with argon *Phys. Rev.* E **68** 066603
[8] Couairon A, Biegert J, Hauri C P, Kornelis W, Helbing F W, Keller U and Mysyrowicz A 2006 Self-compression of ultrashort laser pulses down to one optical cycle by filamentation *J. Mod. Opt.* **53** 75
[9] Odhner J H, Romanov D A and Levis R J 2010 Self-shortening dynamics measured along a femtosecond laser filament in air *Phys. Rev. Lett.* **105** 125001
[10] Polynkin P and Kolesik M 2013 Critical power for self-focusing in the case of ultrashort laser pulses *Phys. Rev.* A **87** 053829
[11] Kosareva O, Kandidov V P, Brodeur A, Chien C Y and Chin S L 1997 Conical emission from laser-plasma interactions in the filamentation of powerful ultrashort laser pulses in air *Opt. Lett.* **22** 1332
[12] Béjot P *et al* 2007 32 TW atmospheric white-light laser *Appl. Phys. Lett.* **90** 151106
[13] Houard A, Jukna V, Point G, Andre Y-B, Klingebiel S, Schultze M, Michel K, Metzger T and Mysyrowicz A 2016 Study of filamentation with a high power high repetition rate ps laser at 1.03 μm *Opt. Express* **24** 7437
[14] Schwarz J, Rambo P, Diels J-C, Kolesik M, Wright E M and Moloney J V 2000 Ultraviolet filamentation in air *Opt. Commun.* **180** 383
[15] Mikalauskas D, Dubietis A and Danielius R 2002 Observation of light filaments induced in air by visible picosecond laser pulses *Appl. Phys.* B **75** 899
[16] Hemmer P R, Miles R B, Polynkin P, Siebert T, Sokolov A V, Sprangle P and Scully M O 2011 Standoff spectroscopy via remote generation of a backward-propagating laser beam *Proc. Natl Acad. Sci.* **108** 3130
[17] Koopman D W and Saum K A 1973 Formation and guiding of high-velocity electrical streamers by laser-induced ionization *J. Appl. Phys.* **44** 5328
[18] Uchida S, Shimada Y, Yasuda H, Motokoshi S, Yamanaka C, Yamanaka T, Kawasaki Z and Tsubakimoto K 1999 Laser-triggered lightning in field experiments *J. Opt. Technol.* **66** 199
[19] Shen H-M 1991 Plasma waveguide: a concept to transfer electromagnetic energy in space *J. Appl. Phys.* **69** 6827
[20] Chen Y-H, Varma S, Antonsen T M and Milchberg H M 2010 Direct measurement of the electron density of extended femtosecond laser pulse-induced filaments *Phys. Rev. Lett.* **105** 215005
[21] Sun Z, Chen J and Rudolph W 2011 Determination of the transient electron temperature in a femtosecond-laser-induced air plasma filament *Phys. Rev.* E **83** 046408
[22] Polynkin P and Moloney J V 2011 Optical breakdown of air triggered by femtosecond laser filaments *Appl. Phys. Lett.* **99** 151103
[23] Polynkin P, Pasenhow B, Driscoll N, Scheller M, Wright E M and Moloney J V 2012 Seeded optically driven avalanche ionization in molecular and noble gases *Phys. Rev.* A **86** 043410
[24] http://jlf.llnl.gov
[25] Point G, Brelet Y, Houard A, Jukna V, Milián C, Carbonnel J, Liu Y, Couairon A and Mysyrowicz A 2014 Superfilamentation in air *Phys. Rev. Lett.* **112** 223902
[26] Xu S, Bernhardt J, Sharifi M, Liu W and Chin S L 2012 Intensity clamping during laser filamentation by TW level femtosecond laser in air and argon *Laser Phys.* **22** 195
[27] Gaarde M B and Couairon A 2009 Intensity spikes in laser filamentation: diagnostics and application *Phys. Rev. Lett.* **103** 043901
[28] Polynkin P 2012 Mobilities of O_2^+ and O_2^- ions in femtosecond laser filaments in air *Appl. Phys. Lett.* **101** 164102
[29] Polynkin P, Kolesik M, Roberts A, Faccio D, Di Trapani P and Moloney J 2008 Generation of extended plasma channels in air using femtosecond Bessel beams *Opt. Express* **16** 15733
[30] Akturk S, Zhou B, Franco M, Couairon A and Mysyrowicz A 2009 Generation of long plasma channels in air by focusing ultrashort laser pulses with an axicon *Opt. Commun.* **282** 129
[31] Kolesik M, Moloney J V and Mlejnek M 2002 Unidirectional optical pulse propagation equation *Phys. Rev. Lett.* **89** 283902
[32] Perelomov A M, Popov V S and Terent'ev M V 1966 Ionization of atoms in an alternating electric field *Sov. Phys.—JETP* **23** 924
[33] Huba J D (ed) 2013 *NRL Plasma Formulary* (Washington, DC: US GPO)
[34] Brabec T and Krausz F 1997 Nonlinear optical pulse propagation in the single-cycle regime *Phys. Rev. Lett.* **78** 3282
[35] Peck E R and Reeder K 1972 Dispersion of air *J. Opt. Soc. Am.* **62** 958
[36] Pitts T A, Luk T S, Gruetzner J K, Nelson T R, McPherson A, Cameron S M and Bernstein A C 2004 Propagation of self-focusing laser pulses in atmosphere: experiment versus numerical simulation *J. Opt. Soc. Am.* B **21** 2008
[37] Wahlstrand J K, Cheng Y-H and Milchberg H M 2012 Absolute measurement of the transient optical nonlinearity in N_2, O_2, N_2o, and Ar *Phys. Rev.* A **85** 043820
[38] Skupin S *et al* 2004 Filamentation of femtosecond light pulses in the air: turbulent cells versus long-range clusters *Phys. Rev.* E **70** 046602
[39] Bergé L *et al* 2004 Multiple filamentation of terawatt laser pulses in air *Phys. Rev. Lett.* **92** 225002
[40] Bespalov V I and Talanov V I 1966 Filamentary structure of light beams in nonlinear liquids *JETP Lett.* **3** 307